BALL SCREW DRIVE SYSTEMS: EVALUATION OF AXIAL AND TORSIONAL DEFORMATIONS

Diego A. Vicente[a]**, Rogelio L. Hecker**[ab]**, Gustavo M. Flores**[a]

[a]*Facultad de Ingeniería, Universidad Nacional de La Pampa, Calle 9 y 110 General Pico, La Pampa, Argentina, vicente@ing.unlpam.edu.ar, http://www.ing.unlpam.edu.ar/*

[b]*CONICET*

Keywords: Screw Drive, Dynamic Model, Vibration Modes, Ritz Series.

Abstract. The ball screw drives are among the most commonly mechanisms used to provide motion in high speed machine tools. The most important factor that affects high speed positioning accuracy is the closed loop bandwidth, which in turn is affected by the structural vibration modes. In recent years, newer strategies have emerged achieving higher control bandwidth, but requiring higher order plant models as well as a better understanding of the system dynamics.

This work presents a dynamic model of a lead screw drive accounting for high frequency modes. The analytical formulation follows a comprehensive approach, where the screw was modeled as a continuous subsystem. The axial and angular displacement fields for this continuous screw were approximated by Ritz series to obtain an approximate N-degree-of-freedom model. Furthermore, it is discussed how to decouple the damping matrix to transform an N-degree-of-freedom system into N one-degree-of-freedom systems, because the advantages that this implies when numerical solution is required.

Then, expressions for the displacement fields in terms of modal coordinates are found and a procedure to compute the axial and angular components of the mode functions is discussed, as well as a numerical procedure to compute the system deformation.

In order to obtain conclusions about the system behavior in the first modes, the axial an angular components of the mode functions are plotted. Then, an analysis based on a comparison with results from others works is presented.

1 INTRODUCTION

Traditionally, the dynamics of each axis in a machine tool is represented as a second order system for which well-known control techniques are applied. In these cases, the rigid body mode is the only mode that must be included into the control system model. However, when designing wider bandwidth positioning systems it becomes necessary to consider additional structural modes. An example is High Speed Machining (HSM), where the feed between the cutting tool and the workpiece increases proportionally to the increased spindle speed (Smith, 1999). This represents a problem, particularly in machining parts that require short and repetitive movements demanding high accelerations profiles. High accelerations profiles excite the machine structure up to high frequencies, thereby exciting the structure vibration modes. Therefore, for HSM, the traditional models must be augmented with higher order dynamics, up to 150 Hz, to assist the controller design, (Hecker and Flores, 2005).

On the other hand, the mechatronical design of industrial servosystems requires, in increasing way, advanced modeling and simulation techniques able to predict the machine dynamics, which may interact in a non-intuitive way with the control actions.

Smith (1999) used finite elements modeling to analyze a ball-screw positioning system of a high-speed milling machine. From the model the author predicts the natural frequencies and the shapes of the first vibration modes. In a similar way, Erkorkmaz and Kamalazadeh (2006) used a finite element model to study the torsional dynamics of the ball screw mechanism, from which it was predicted the natural frequencies and shapes of the first torsional modes.

A more comprehensive model was presented by Varanasi (2002), Varanasi and Nayfeh (2001, 2004), where an accurate model for the first axial mode was obtained. The author considered the screw as a distributed parameter system and assumed that the axial and torsional displacement fields vary linearly with the axial coordinate of the screw. Although the model follows a general formulation, only the frequency of the first mode was predicted due to the assumptions considered in the solution.

Vicente et al. (2007) presented a dynamic model of a feed drive servomechanism accounting for high frequency modes. The formulation follows a comprehensive approach with the screw modeled as a continuous subsystem, where the axial and torsional dynamics are characterized by continuous functions denominated displacement fields. The displacement field for the screw was approximated by Ritz series to find a finite dimensional model.

The aim of this work is to propose a way to evaluate the system dynamics of a ball-screw-drive servosystem based on the model presented by Vicente et al. (2007). First, the model is constructed using power balance method and using Ritz series to represent the axial and angular displacement fields. After that, expressions for the displacement fields in terms of modal coordinates are found from the model solutions. A general procedure to evaluate numerically the displacement field is discussed as well as a procedure to compute the axial and angular components of the mode functions. Finally, the mode functions of the first modes are plotted and analyzed.

2 SERVOMECHANISM MODEL

A typical feed drive servomechanism for precision positioning, such those found in machine tools, is shown in Figure 1. It consists of a ball-screw assembled to the machine base by rotary bearings, which is driven by an electric-servomotor through a flexible coupling. The ball-nut is attached to the carriage that is constrained to move axially on linear bearings and guideways.

The schematic model considered here is presented in Figure 2, in which the screw is solely

a continuous system, whereas the remaining elements are assumed in the lumped form. In these conditions, the screw can be considered as a straight bar with three fundamental types of deformations: axial deformation, by traction or compression, angular deformation, by torsion, and flexural deformation. Flexure is discarded, assuming the screw is suitably mounted in the servomechanism and then minimizing buckling due to non-concentric forces produced by misalignments.
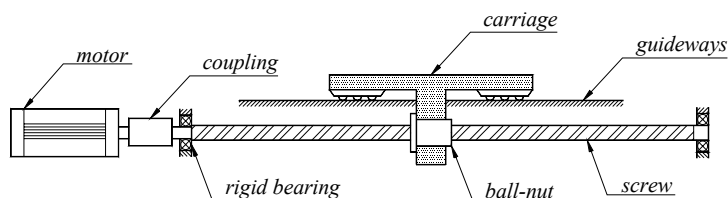

Figure 1: Ball-screw feed system

In this way, the continuous deformation can be represented by an axial displacement using a field function $u(x,t)$ and by an angular displacement using $\theta(x,t)$. This continuous portion is characterized by mass-density ρ, cross-section A, moment of inertia J_t, length L, Young's modulus E, Poisson's modulus G, and screw lead l (also cited as transmission ratio).

The elements assumed in the lumped form are the rotor of the electric motor with moment of inertia J_m, the flexible coupling with moment of inertia J_a and stiffness k_a, the rigid bearing with stiffness k_b, and the carriage with mass m_c.
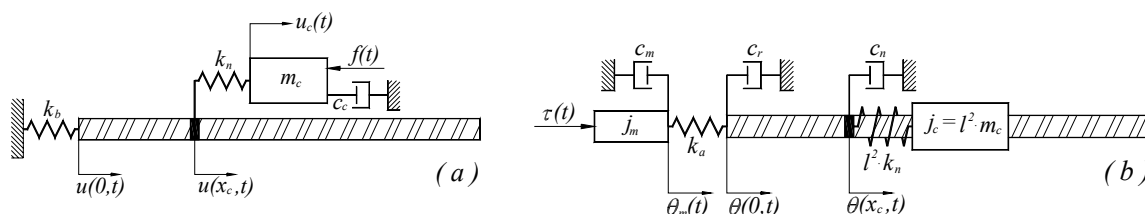

Figure 2: Schematic of the ball-screw feed system. (a) Axial. (b) Angular.

As Figure 2 shows, in addition to the generalized coordinates from the continuous portion, there are two additional generalized coordinates, one to describe the carriage position $u_c(t)$ and another to describe the rotor angular position $\theta_m(t)$.

2.1 Power balance fromulation

A convenient approach to obtain motion equations in this kind of systems is the power balance method based on energy and work formulation, (Ginsberg, 2001).

The general formulation of the power balance law for a vibratory system is

$$\dot{T} + \dot{V} = P_{in} + P_{dis} \qquad (1)$$

where T and V are the kinetic and potential energy of the system, whereas P_{in} and P_{dis} are the power input and the power dissipation in the system.

Using the defined variables, the kinetic energy can be computed as follows

$$T = \frac{1}{2} m_c \dot{u}_c(t)^2 + \frac{1}{2} J_m \dot{\theta}_m(t)^2 + \frac{1}{2} J_a \left(\frac{\dot{\theta}_m(t) + \dot{\theta}(0,t)}{2} \right)^2$$
$$+ \frac{1}{2} \rho J_t \int_0^L \dot{\theta}(x,t)^2 \, dx + \frac{1}{2} \rho A \int_0^L \dot{u}(x,t)^2 \, dx \qquad (2)$$

where the first and the second terms represent the contributions from the mass of the carriage and the inertia of the rotor respectively. The third term is the energy from the flexible coupling, for which an average speed between the angular velocity of the rotor and the angular velocity of the screw in $x = 0$ was considered. The fourth and the fifth terms represent the kinetic energy from the distributed rotary inertia and the distributed linear inertia of the screw respectively.

The potential energy stored in the elastic parts of the system can be computed according to

$$V = \frac{1}{2} k_b u(0,t)^2 + \frac{1}{2} k_a \left[\theta_m(t) - \theta(0,t) \right]^2 + \frac{1}{2} k_n \delta_n^2$$
$$+ \frac{1}{2} J_t G \int_0^L \left(\frac{d\theta(x,t)}{dx} \right)^2 dx + \frac{1}{2} E A \int_0^L \left(\frac{du(x,t)}{dx} \right)^2 dx \qquad (3)$$

where the first and second terms correspond to the potential energy in the rigid bearing and flexible coupling respectively. Similarly, the third term corresponds to the potential energy stored in the ball-nut, where k_n is the nut's stiffness coefficient and δ_n is the axial deformation in the nut. Although the elastic deformations produced by the normal contact forces have axial and radial components (Wei and Lin, 2003), only the axial component influences the axial displacement field.

Therefore, the interface axial deformation can be expressed as

$$\delta_n = u_c(t) - \left(u(x_c,t) + \theta(x_c,t) l \right) \qquad (4)$$

that denotes the difference between the absolute position of the carriage, $u_c(t)$, and the absolute position of the screw at the interface-point coordinate x_c. It is important to notice that Eq. (4) involves axial and torsional displacements together, producing a coupling of both displacements, a fact that forbids each field to be treated separately. Alternatively, the fourth and the fifth terms of Eq. (3) represent the potential energy stored in the continuous portion of the system, the screw, by torsional and axial displacements.

The power input to the system results in

$$P_{in} = \tau_m \dot{\theta}_m(t) - \tau_f \dot{\theta}(x_c,t) - f_c \dot{u}_c(t) \qquad (5)$$

where the first term is the power input from the motor, the second term is the coulomb friction dissipation in the ball-nut due to the friction torque τ_f, and the third term represents the power required to move the carriage at the velocity $\dot{u}_c$ against a disturbance force f_c. Note that f_c is a general variable to account for external forces actuating on the carriage, which can include machining forces and coulomb friction forces in guideways.

Alternatively, the power dissipation in the system due to viscous friction can be expressed as follows

$$P_{dis} = \int_0^L \gamma\, E\, A \left(\frac{du(x,t)}{dx} \right)^2 dx + \int_0^L \gamma\, G\, J_t \left(\frac{d\theta(x,t)}{dx} \right)^2 dx \tag{6}$$

$$+ c_m\, \dot{\theta}_m(t)^2 + c_b\, \dot{\theta}(0,t)^2 + c_n\, \dot{\theta}(x_c,t)^2 + c_c\, \dot{u}_c(t)^2$$

The first two terms represent the power dissipation due to the viscoelastic behavior of the continuous portion. The other four terms represent the power dissipation in rotor bearings, rigid bearing, ball-nut, and guideways, respectively. Therefore, the coefficients c_m, c_b, c_n and c_c are the viscous friction coefficients of these elements.

All the above equations depend on the displacement fields $u(x,t)$ and $\theta(x,t)$ that must be formulated. A rigorous treatment of vibrations of continua requires the solution of exact field equations, that is to say, equations governing deformations that depend on time and spatial coordinates. An alternative and convenient method is the approximation of these equations by a Ritz series as is described in the next section.

2.2 Basis functions selection and close loop form system representation

The deformation in a continuous general system can be represented by a displacement field $u(x,t)$ that is a function of the time and the spatial coordinates. The Ritz series method, (Ginsberg, 2001), also known as method of assumed modes, uses a series expansion to approach the displacement field as follows

$$u(x,t) = \sum_{j=1}^N \psi_j(x) q_j(t) \tag{7}$$

where the basis functions $\psi_j(x)$ represent the displacement field as a function of the x coordinate and the coefficients $q_j(t)$ represent the instant contribution of $\psi_j(x)$ over the displacement field.

From a mathematical perspective, Eq. (7) maps a continuous function over an N-dimensional space whose directions are the functions ψ_j, so these functions are called basis functions. The coefficients q_j represent projections of u in the direction of each basis functions. The approach using the Ritz series will be a discrete model with N degree of freedom that approximates the behavior of a system with infinites degrees of freedom.

The basis functions must fulfill certain conditions to obtain a valid formulation of the Ritz series. All basis functions must be continuous, linearly independent and must satisfy the geometric boundary conditions (Ginsberg, 2001). In this way a suitable axial field equations can be constructed using cosine basis functions.

$$u(x,t) = \sum_{j_u=1}^{N_u} \cos\left(\alpha \frac{x}{L} \right) q_{j_u}(t) \tag{8}$$

where $\alpha = (j_u - 1)\pi$. The first term in the series (with $j_u = 1$) is the unitary function that represent the rigid body motion which is kinematically admissible for this system. This is because the screw is attached to the base by the bearing, which is modeled as a lumped spring, as Figure 2a shows. Therefore, although the rigid body motion would not actually occur, it is advisable to introduce a unitary function to account for stiffness differences between the screw and the rigid bearing (Ginsberg, 2001).

It is more obvious that the screw has a rigid body motion for the angular displacement; then, the displacement field to describe rotation in the screw can be represented by

$$\theta(x,t) = \sum_{j_\theta=1}^{N_\theta} \cos\left(\alpha \frac{x}{L}\right) q_{j_\theta}(t) \tag{9}$$

where $\alpha = (j_\theta - 1)\pi$.

The number of terms N_u and N_θ, can be selected by studying the convergence of the model solutions as will be discussed later.

The power balance method requires expressions in terms of generalized coordinates, which can be obtained combining de Ritz series with the expressions for T, V, P_{in} and P_{dis}. This can be done, replacing Eq. (8) and Eq. (9) in the expression for the kinetic energy, Eq. (2), potential energy, Eq. (3), power input, Eq. (5), and power dissipation, Eq. (6). In order to account for all combinations when the series expansion is substituted into the energy and power expressions, different indices j and n are used to form each term, (Ginsberg, 2001). Therefore, the kinetic energy can be expressed in a general form as

$$T = \frac{1}{2} \sum_{j=1}^{N} \sum_{n=1}^{N} M_{jn} \dot{q}_j \dot{q}_n \tag{10}$$

where the inertia coefficients, M_{jn}, are calculated as

$$M_{jn} = M_{nj} = \int_0^L \rho A \psi_j \psi_n \, dx + \sum m \psi_j(x_m) \psi_n(x_m) \tag{11}$$

In the same way, it is possible to obtain an expression for the potential energy as

$$V = \frac{1}{2} \sum_{j=1}^{N} \sum_{n=1}^{N} K_{jn} q_j q_n \tag{12}$$

where the stiffness coefficients, K_{jn}, are given by

$$K_{jn} = K_{nj} = \int_0^L E A \frac{d\psi_j}{dx} \frac{d\psi_n}{dx} dx + \sum k \psi_j(x_k) \psi_n(x_k) \tag{13}$$

Also, the dissipated energy can be expressed as

$$P_{dis} = \sum_{j=1}^{N} \sum_{n=1}^{N} C_{jn} \dot{q}_j \dot{q}_n \tag{14}$$

where the viscosity coefficients, C_{jn}, are

$$C_{jn} = C_{nj} = \int_0^L \gamma E A \frac{d\psi_j}{dx} \frac{d\psi_n}{dx} dx + \sum c \psi_j(x_c) \psi_n(x_c) \tag{15}$$

Finally, it is possible to obtain an expression for input energy as follows

$$P_{in} = \sum_{j=1}^{N} Q_j \dot{q}_j \tag{16}$$

where the generalized forces, Q_j, are given by

$$Q_j = \int_0^L f_x \psi_j \, dx + \sum F \psi_j(x_F, t) \tag{17}$$

where the f_x represents a distributed force and F a concentrated force.

The benefit of using the Power Balance methodology is the convenient way to find the

dynamic equations from the energy formulation. After the coefficients and the generalized forces are calculated as described above, they can be used to write the dynamic equations in a matrix form as

$$[M]\{\ddot{q}\} + [C]\{\dot{q}\} + [K]\{q\} = \{Q\} \tag{18}$$

where each matrix is formed using the calculated coefficients; therefore, the solution of this system will be a function of the generalized coordinates.

As Figure 2 shows, in addition to the generalized coordinates from the continuous portion, there are two additional generalized coordinates, one to describe the carriage position u_c and other one to describe the rotor angular position θ_m. Thus the total system order is $N = N_U + N_\Theta$, with $N_U = N_u + 1$ and $N_\Theta = N_\theta + 1$.

The solution of the eigenvalue problem $[[K] - \omega_j^2[M]]\{\Phi_j\} = \{0\}$ related to Eq. (18) gives N eigensolutions, each of one features a natural frequency ω_j and a normal mode $\{\Phi_j\}$.

The convergence of the model solution can be analyzed comparing the changes in each natural frequency value from the solutions for different series extensions. As the number of terms increases, more high frequency modes can be estimated and each particular frequency approaches a stationary value monotonically from higher values. It was observed that the first four modes present a favorable approximation using only 3 terms in Eq. (8) and (9), (Vicente et al. 2007).

2.3 Decoupled system equations

The Eq. (18) represents a system of N differentials equations coupled by the off diagonal elements of the inertia, stiffness and damping matrices, making difficult to find the solutions for generalized coordinates.

Nevertheless, considering the uncoupled nature of the stiffness and inertia matrices, applying the modal transformation $\{q\} = [\Phi]\{\eta\}$, Eq. (18) results in

$$\{\ddot{\eta}\} + [\Phi]^{\mathrm{T}}[C][\Phi]\{\dot{\eta}\} + \left[\mathrm{diag}\left(\omega^2\right)\right]\{\eta\} = [\Phi]^{\mathrm{T}}\{Q\} \tag{19}$$

where $\{\eta\}$ is the vector formed by the modal coordinates, $[\Phi]$ is a matrix formed from the normalized eigenvectors $[\Phi] = [\{\Phi_1\} \ldots \{\Phi_N\}]$ and $[\mathrm{diag}(\omega^2)]$ is a diagonal matrix formed by the square natural frequencies.

As can be seen, the modal equations are only coupled by the matrix $[\Phi]^{\mathrm{T}}[C][\Phi]$. However, the off-diagonal elements of $[\Phi]^{\mathrm{T}}[C][\Phi]$ can be discarded in systems where damping is light. Thus for a particular η_j the equivalent damping ratio can be obtained replacing the coefficient $[[\Phi]^{\mathrm{T}}[C][\Phi]]_{jj}$ by $2\omega_j\zeta_j$, resulting in

$$\ddot{\eta}_j + 2\zeta_j\omega_j\dot{\eta}_j + \omega_j^2\eta_j = \{\Phi_j\}\{Q\}$$

$$\zeta_j = \frac{1}{2\omega_j}\left[[\Phi]^{\mathrm{T}}[C][\Phi]\right]_{jj} \tag{20}$$

The light damping approximation is acceptable when the equivalent damping ratios ζ_j are found to be less than 0.1 (Ginsberg, 2001). In ball-screw servosystems, the damping is provided by viscous forces in the screw and servomotor bearings, the nut, and the guide ways, so the structural modes tend to have low damping ratios. In Smith (1999) the equivalent damping ratio of the first mode was found to be 0.1, whereas in the others modes it was about 0.01. In Varanasi (2002), the damping ratio for the first mode was found to be 0.02.

According to this, the light damping approach seems to be a good approximation to decouple Eq. (19) in this kind of systems.

To decouple the system equations is convenient to find the solution for modal coordinates. As Eq. (20) shows, the differential equation for each modal coordinate is like a one-degree-of-freedom oscillator with unitary mass. In other words, the N-degree-of-freedom system was converted into N one-degree-of-freedom systems whose solution is well known.

3   EXPRESSIONS FOR THE DISPLACEMENT FIELDS

Tasks such as system identification and controller design for HSM, require a better knowledge of the system dynamics, particularly at higher frequencies that conventional machines. In this way, some researchers have developed finite elements models from which the mode shapes can be predicted (Smith, 1999; Erkorkmaz and Kamalzadeh, 2006). Alternatively, this work proposes to obtain expressions to allow the numerical evaluation of the displacement fields, from the solution of the general model presented in previous sections.

An alternative form to write the displacement field, as is done in Eq (7), is to use matrix notation as follows

$$u(x,t) = [\psi]\{q\} \tag{21}$$

where $[\psi]$ is a row formed from the basis functions $[\psi] = [\psi_1 \dots \psi_N]$. Generally, the matrix representation may be advantageous in front of the summation form for computational implementation.

Since damping is light in ball-screw systems and Eq. (19) can be decoupled, it is convenient to express the deformation fields in terms of modal coordinates, which can be done by simply substitution of modal transformation $\{q\} = [\Phi]\{\eta\}$ into Eq. (21). Then, the displacement field in terms of modal coordinates results in

$$u(x,t) = [\psi][\Phi]\{\eta\} = [\Psi]\{\eta\} \tag{22}$$

where $[\Psi]$ is a row formed by the functions $\Psi_j = [\psi]\{\Phi_j\}$ known as mode functions.

As the elements of the mode vector $\{\Phi_j\}$ gives the proportions between the various generalized coordinates, the mode function Ψ_j gives the deformation proportions as a function of the x coordinate, in the jth mode. On the other hand, the η_j represents the mode contribution to the displacement field.

3.1 Computer implementation

The matrix form of Eq. (22) is particularly useful for computational implementation. For example, to evaluate $u(x,t)$ at a succession of n points along the system, that is $x = \{x_1 \dots x_n\}$, the matrix $[\Psi] = [\psi][\Phi]$ will be a rectangular array having n rows and N columns. Computation of the product values $[\Psi]\{\eta\}$ would yield a column whose elements are the displacements at the various x_n corresponding to the instant t_i at which $\{\eta\}$ is evaluated. Mathematically, this can be expressed as

$$\begin{bmatrix} u(x_1,t_i) \\ u(x_2,t_i) \\ \vdots \\ u(x_n,t_i) \end{bmatrix} = \begin{bmatrix} \Psi_1(x_1) \cdots \Psi_N(x_1) \\ \Psi_1(x_2) \cdots \Psi_N(x_2) \\ \vdots \qquad \vdots \\ \Psi_1(x_n) \cdots \Psi_N(x_n) \end{bmatrix} \begin{bmatrix} \eta_1(t_i) \\ \eta_2(t_i) \\ \vdots \\ \eta_N(t_i) \end{bmatrix} \tag{23}$$

According to this, the procedure to obtain an expression for the displacement field requires the construction of the mode functions [Ψ] and to solve Eq. (20) to obtain the solution for the modal coordinates $\{\eta\}$. In the most general case, the solution for $\{\eta\}$ will depend on initial conditions $\{\eta(0)\}$ and external forces applied on the system $\{Q\}$.

Nevertheless, the first step in the analysis of the system behavior is to find and draw the mode functions, which are own of the system and, therefore, they depend neither on the particular conditions nor on the external excitations. Although, the mode functions do not represent the absolute deformations, they indicate how the deformation is distributed along the system in each mode. This is the main focus of the remaining of this work.

3.2 Axial and angular components of the mode functions

Since the system undergoes two types of deformation, it is clear that in the most general case, each vibration mode is composed of two kinds of movements: axial and angular. According to this, it can be said that each mode function will have two components. One of them associated to axial displacement, that will be identified as Ψ_{uj} and other one associated to the angular displacements, identified as $\Psi_{\theta j}$.

To compute the axial and angular components of the mode functions, it is necessary to distinguish, in each mode vector $\{\Phi_j\}$, the elements corresponding to each one of the generalized coordinates. In this sense, if the generalized coordinates vector $\{q\}$ has the following arrange

$$\{q\} = \left\{ q_{u_1} \cdots q_{u_{N_u}} \ q_{\theta_1} \cdots q_{\theta_{N_\theta}} u_c \ \theta_m \right\}^{\mathrm{T}} \qquad (24)$$

each mode vector $\{\Phi_j\}$ can be written as

$$\left\{\Phi_j\right\} = \left\{ \Phi_{u_1} \cdots \Phi_{u_{N_u}} \Phi_{\theta_1} \cdots \Phi_{\theta_{N_\theta}} \Phi_{u_c} \Phi_{\theta_m} \right\}^{\mathrm{T}} \qquad (25)$$

Therefore, the first N_u elements of $\{\Phi_j\}$ are associated with the axial displacements and the following N_θ elements of $\{\Phi_j\}$ are associated with the angular displacements. Whereas, the last two elements of $\{\Phi_j\}$, Φ_{ucj} and $\Phi_{\theta mj}$, are the elements describing the carriage displacement and the rotor-motor angular displacement, respectively.

In this way, the axial component of jth mode function can be constructed from the basis functions used to describe the axial field and the first N_u elements of $\{\Phi_j\}$ as follows

$$\Psi_{u_j}(x) = \left[\psi_{u_1}(x)\psi_{u_2} \ldots \psi_{u_{N_u}}(x) \right] \begin{Bmatrix} \Phi_{u_j} \\ \vdots \\ \Phi_{N_{u_j}} \end{Bmatrix} \qquad (26)$$

Similarly, the angular component of jth mode function results in

$$\Psi_{\theta_j}(x) = \left[\psi_{\theta_1}(x)\psi_{\theta_2} \ldots \psi_{\theta_{N_\theta}}(x) \right] \begin{Bmatrix} \Phi_{\theta_j} \\ \vdots \\ \Phi_{N_{\theta_j}} \end{Bmatrix} \qquad (27)$$

According to Eq (26) and (27), to find the axial and angular components of the mode functions, it only requires to identify the elements, from $\{\Phi_j\}$, associated with each type of

deformation. It is important to state that the arrangement of the mode vector will depend on arrangement of the generalized coordinates in Eq. (18).

In this system, a complete description of the axial shape in the jth mode includes the Φ_{ucj} element, accounting for the carriage motion, in addition to the axial component of mode function. In the same way a complete description of the angular shape includes $\Phi_{\theta mj}$, accounting for the rotor motion, in addition to the angular component of the mode function.

4   MODE FUNCTIONS

Figures 3a and 3b show the axial and angular components of the mode functions for the first four modes of a ball screw drive. Also, in Figure 3a, the motion of the carriage was described in each mode as a point value Φ_{ucj} plotted at $x = x_c$. Similarly, in Figure 3b, the motion of the motor rotor was described by $\Phi_{\theta mj}$ plotted at $x = 0$.

The mode functions were obtained according to Eq. (26) and (27) in which the mode vectors correspond to the system solution with the physical parameters in Table 1 and the particular carriage position $x_c = 0.5L$. The number of terms included into Eq. (8) and (9) were $N_u = N_\theta = 4$.

As can be seen from the first mode, Ψ_{u1} and $\Psi_{\theta 1}$, the screw is not experiencing any kind of deformation; because, this is the rigid body mode corresponding to the rigid rotation of the rotor, the coupling and the screw. This is also confirmed by the ratio between the carriage motion value Φ_{uc1} and the angular motion value $\Psi_{\theta 1}$, which is exactly the transmission ratio l. The rigid body mode is the only mode that provides useful motion, whereas the others correspond to small displacements around the position determined by the rigid motion.

Although each mode has axial and angular deformations, it is important to classify the vibration modes either as axial or torsional, according to the predominant deformation. The knowledge of each mode character is convenient to identify the stiffness and inertia parameters that have greater influence on each mode, which can be useful for design purposes.

The mode characterization from the comparison of axial and angular components of the mode functions is somewhat subjective. It requires a match between different kinds of deformations, which implies an implicit valuation of when one kind of deformation is substantially less significant compared to the others.

Nevertheless, it can be seen that the amplitude of axial components Ψ_u diminishes as the mode number grows, whereas the angular component amplitude Ψ_θ increases. It is important to point out that the absolute deformation in each mode depends on the mode contribution η_j, as Eq. (22) indicates. An increment or decrement of the amplitude in the mode function, from one mode to another, does not necessarily means that the deformation increases or decreases in the same proportion. However, as the axial and angular deformation in each mode depends on the same contribution η_j, a relative increment of one component respect to the other one, means a greater predominance of this type of deformation in the mode.

In this way, in the second mode, which is the first vibration mode, the axial component amplitude Ψ_{u2} has the greatest values compared to their homologues, whereas the angular $\Psi_{\theta 2}$ has the smaller one. In addition, the displacement of the carriage Φ_{uc2} has the largest value, which is consistent with Smith (1999), in which the second mode was described as an axial mode where de carriage is connected to ground by the axial stiffness of the ball screw, ball nut and the rigid bearing. The axial dominance of this mode also agrees with Vicente et al. (2008), who compared the natural frequencies values from the solutions of axial and torsional decoupled models, with the values from the coupled model as represented by Eq. (18).

As can be also seen from Figure 3, in the third mode, the amplitude of the angular component increases considerably, whereas the axial decreases and the axial displacement of the carriage is substantially lower. Nevertheless, the axial mode function amplitude has a significant value. This agrees with results in Vicente et al. (2008), in which was observed that in some modes exists a strong coupling between the axial and angular deformations, and the coupling increases as the trasnmition ratio increases. It means that the axial and angular deformations are both important. About the character of this mode, Vicente et al. (2008) concluded that it is essentially a torsional mode for low transmission ratios and becomes coupled as the transmission ratio increases.
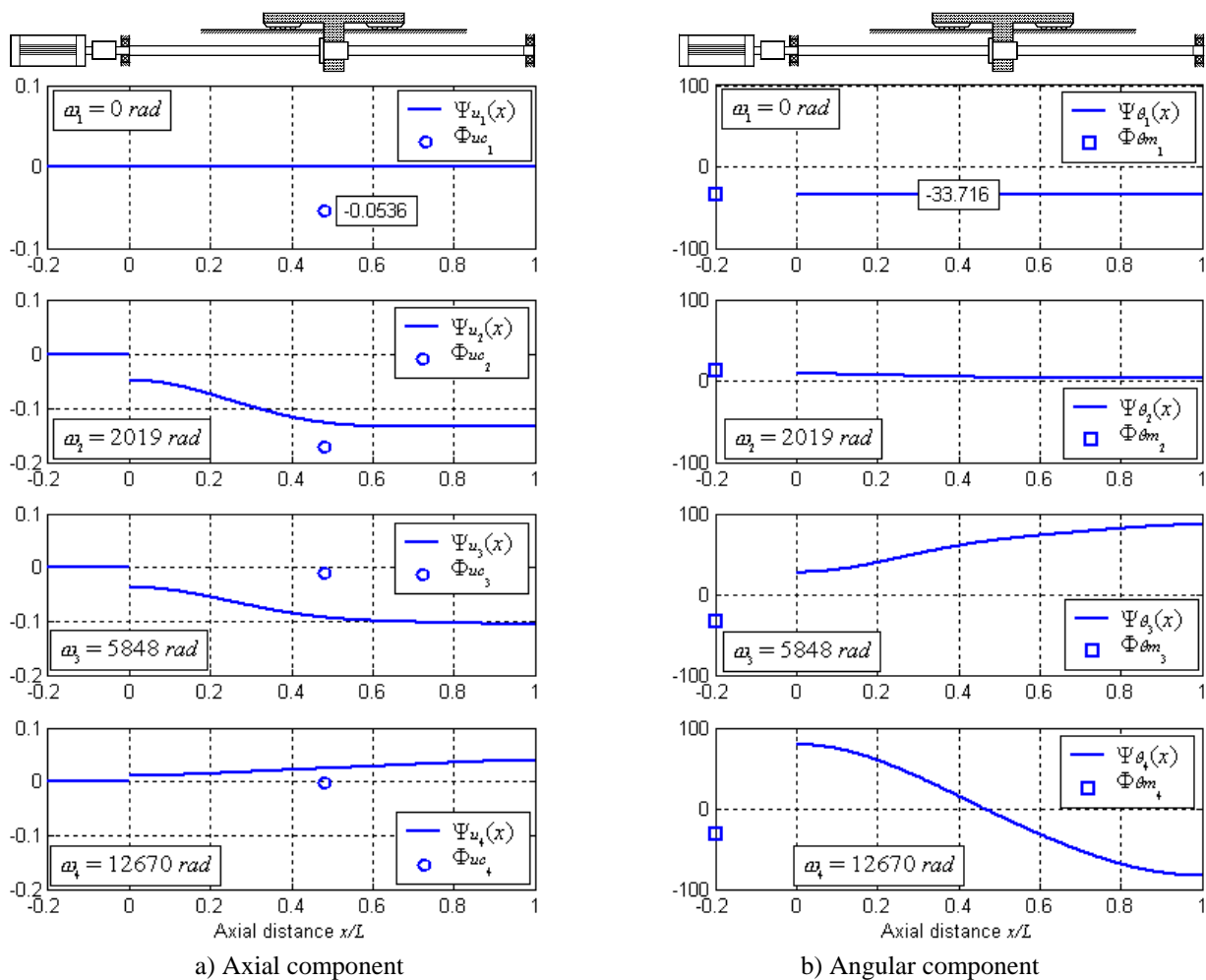

Figure 3 : Axial an Angular components of the mode functions.

Finally, in the fourth mode, the amplitude of the angular component shows the largest values, whereas the axial, as well as the displacements of the carriage, are very small. For this mode Vicente et al. (2008) concluded that this is a clearly torsional mode.

On the other hand, the knowledge of system behavior in each mode can be very useful for identification purposes, especially at high frequencies. From Figure 3 it can be seen that a convenient point to perform measurements, to identify the second mode, is the carriage position u_c, because this is the point showing the largest deformation in this mode. Similarly, the angular position at the end of the screw $\theta(x = L)$ can be a suitable point of measurement to identify the third and fourth modes.

ρ	7850	[kg/m^3]
E	2,06x10^{11}	[N/m^2]
G	8,1x10^{10}	[N/m^2]
A	4,22x10^{-4}	[m^2]
J_t	2,8x10^{-8}	[m^4]
L	0,743	[m]
J_a	3,8x10^{-4}	[kg m^2]
J_m	2,6x10^{-4}	[kg m^2]
m_c	30	[kg]
k_n	4,3x10^8	[N/m]
k_b	4,5x10^8	[N/m]
k_a	5200	[Nm/rad]
l	1,59x10^{-3}	m/rad

Table 1: Parameter values used in the model.

Furthermore, the knowledge of the mode functions can be very important for certain control application. For example, if the carriage position u_c is the variable to be controlled, it is clear that the second mode is the one that contributes with greatest elastic deformations. Therefore, to enhance the final linear positioning bandwidth it is necessary to compensate this mode, (Kamalazadeh and Erkorkmaz, 2007).

5 CONCLUSIONS

A finite dimensional model of a ball-screw feed-drive system is presented, where Ritz series were used to approximate the continuous field displacements of the ball screw subsystem. The model was used to predict the natural frequencies and to evaluate the system deformation based on the mode functions.

Since this kind of systems has very low damping, the system equations in modal coordinates can be decoupled. In this way a procedure to compute the deformation fields in terms of modal coordinates was discussed, based on the mode functions and modal coordinates.

As the system experience axial and angular deformations, the mode functions will have two components in each mode. Thus, a way to obtain the axial and angular components is proposed and then applied to find and to analyze the shapes of the first four modes.

From the components of the mode functions can be seen that the first mode is the rigid body mode, corresponding to the rigid rotation of the screw. In the second mode, the axial deformation has the largest values as well as the largest carriage displacement. The third mode is highly coupled, whereas the fourth mode has an angular predominance.

RFERENCES

Erkorkmaz, K. and Kamalazadeh, A., High Bandwidth Control of Ball Screw Drives, *Annals of the CIRP* vol. 55/1, 2006.

Ginsberg, J. H., *Mechanical and Structural Vibrations Theory and Applications*, 1st edition, John Wiley & Sons, 2001.

Hecker, R. L. and Flores G. M., A Review of Machine-Tools Servocontrol Level, *XI RPIC*, Río Cuarto, Córdoba, 2005.

Kamalazadeh, A. and Erkorkmaz, K., Compensation of Axial Vibrations in Ball Screw Drives, *Annals of the CIRP* vol. 56/1, 2007.

Smith, D. A., Wide bandwidth control of high-speed milling machine of feed drives, *PhD dissertation*, University of Florida, 1999.

Varanasi, K. K. and Nayfeh, S. A, Modeling, Identification, and Control of Ballscrew Drives, *American Society for Precision Engineering 16th Annual Meeting*, 25: 139-142, Crystal City, Virginia, 2001.

Varanasi, K. K., On the Design of a Precision Machine for Closed-Loop Performance, *MS thesis*, Massachusetts Institute of Technology, Cambridge, Massachusetts, 2002.

Varanasi, K. K. and Nayfeh, S. A., The Dynamics of Lead-Screw Drives: Low-Order Modeling and Experiments, *Journal of Dynamic Systems, Measurement, and Control*, ASME, 126: 388-396, 2004.

Vicente, D. A., Hecker, R. L. and Flores, G., Dynamic Modeling of Lead Screw Drives using Ritz Series" *XII RPIC*, Río Gallegos, Santa Cruz, 2007.

Vicente, D. A., Hecker, R. L. and Flores, G., Vibration Modes Characterization in a Lead Screw Drive, *Proceedings of MUSME, the International Symposium on Multibody Systems and Mechatronics*, San Juan, Argentina, Paper n. 23-MUSME08.

Wei, Ch. Ch. and Lin, J. F., Kinematic Analysis of the Ball Screw Mechanism Considering Variable Contact Angles and Elastic Deformation, *Journal of Mechanical Design*, 125: 717-733, 2003.